Distinct properties of Ca^{2+}–calmodulin binding to N- and C-terminal regulatory regions of the TRPV1 channel

Sze-Yi Lau, Erik Procko, and Rachelle Gaudet

Department of Molecular and Cellular Biology, Harvard University, Cambridge, MA 02138

Transient receptor potential (TRP) vanilloid 1 (TRPV1) is a molecular pain receptor belonging to the TRP superfamily of nonselective cation channels. As a polymodal receptor, TRPV1 responds to heat and a wide range of chemical stimuli. The influx of calcium after channel activation serves as a negative feedback mechanism leading to TRPV1 desensitization. The cellular calcium sensor calmodulin (CaM) likely participates in the desensitization of TRPV1. Two CaM-binding sites are identified in TRPV1: the N-terminal ankyrin repeat domain (ARD) and a short distal C-terminal (CT) segment. Here, we present the crystal structure of calcium-bound CaM (Ca^{2+}–CaM) in complex with the TRPV1-CT segment, determined to 1.95-Å resolution. The two lobes of Ca^{2+}–CaM wrap around a helical TRPV1-CT segment in an antiparallel orientation, and two hydrophobic anchors, W787 and L796, contact the C-lobe and N-lobe of Ca^{2+}–CaM, respectively. This structure is similar to canonical Ca^{2+}–CaM-peptide complexes, although TRPV1 contains no classical CaM recognition sequence motif. Using structural and mutational studies, we established the TRPV1 C terminus as a high affinity Ca^{2+}–CaM-binding site in both the isolated TRPV1 C terminus and in full-length TRPV1. Although a ternary complex of CaM, TRPV1-ARD, and TRPV1-CT had previously been postulated, we found no biochemical evidence of such a complex. In electrophysiology studies, mutation of the Ca^{2+}–CaM-binding site on TRPV1-ARD abolished desensitization in response to repeated application of capsaicin, whereas mutation of the Ca^{2+}–CaM-binding site in TRPV1-CT led to a more subtle phenotype of slowed and reduced TRPV1 desensitization. In summary, our results show that the TRPV1-ARD is an important mediator of TRPV1 desensitization, whereas TRPV1-CT has higher affinity for CaM and is likely involved in separate regulatory mechanisms.

The Journal of General Physiology

INTRODUCTION

Transient receptor potential (TRP) vanilloid 1 (TRPV1) is well recognized as a polymodal molecular pain receptor that responds to a wide range of stimuli including noxious heat >43°C, chemical agonists, and protons (Caterina et al., 1997; Tominaga et al., 1998). TRPV1 responses to these stimuli signal the exposure to extreme temperature or tissue damage to elicit appropriate protective mechanisms. TRPV1 is well characterized for its activation by capsaicin, a naturally occurring compound found in chili peppers (Caterina et al., 1997). Prolonged activation of TRPV1 with capsaicin results in acute desensitization, where TRPV1 activity decreases during the course of stimulation. In contrast, repeated stimulation of TRPV1 results in tachyphylaxis, where TRPV1 activation decreases with successive stimulation followed by loss of response to any subsequent stimuli.

TRPV1 belongs to the TRP superfamily of nonselective cation channels with high relative permeability for Ca^{2+} (Caterina et al., 1997). All TRP channels share a similar topology comprising six predicted helical transmembrane segments (S1–S6) and large N- and C-terminal (CT) cytosolic regions for integrating cellular signaling with channel activity (Gaudet, 2008). The N-terminal region of TRPV1 contains an ankyrin repeat domain (ARD), of which a structure is available (Lishko et al., 2007). The cytoplasmic C terminus, of unknown structure, contains multiple sites for interactions with modulatory factors. TRPV1 functions as a tetramer, with S5–S6 forming the pore through which ion conduction occurs. Opening of TRPV1 after channel activation allows the influx of cations, including Ca^{2+}, into the cell.

The intracellular Ca^{2+} concentration is kept as low as 10^{-7} M compared with a high external Ca^{2+} concentration up to 10^{-3} M (Yamniuk and Vogel, 2004). The steep Ca^{2+} concentration gradient across the membrane in combination with the high relative permeability of TRPV1 for Ca^{2+} ensures rapid Ca^{2+} influx into the cells upon TRPV1 activation. However, intracellular calcium

Correspondence to Rachelle Gaudet: gaudet@mcb.harvard.edu

Erik Procko's present address is Howard Hughes Medical Institute and Dept. of Biochemistry, University of Washington, Seattle, WA 98195.

Abbreviations used in this paper: ARD, ankyrin repeat domain; CaM, calmodulin; CaMKK, CaM-dependent kinase kinase; CT, C terminal; MARCKS, myristoylated alanine-rich C kinase substrate; MBP, maltose-binding protein; PIP_2, phosphatidylinositol-4,5-bisphosphate; SEC, size-exclusion chromatography; TRP, transient receptor potential; TRPV1, TRP vanilloid 1.

The Rockefeller University Press $30.00
J. Gen. Physiol. Vol. 140 No. 5 541–555
www.jgp.org/cgi/doi/10.1085/jgp.201210810

homeostasis is crucial for normal cell function (Han et al., 2007), and continuous capsaicin activation of cells expressing TRPV1 or stimulation of TRPV1 with the potent agonist resiniferatoxin results in severe cytotoxicity and cell death (Caterina et al., 1997; Karai et al., 2004). Ca^{2+} ions are involved in various cellular processes including several Ca^{2+}-dependent desensitization mechanisms identified for TRPV1. One is the Ca^{2+}-dependent recruitment of the calcineurin phosphatase to TRPV1 via a scaffolding protein, promoting the dephosphorylation and dampening of TRPV1 activity (Docherty et al., 1996; Mohapatra and Nau, 2005; Zhang et al., 2008). Similarly, Ca^{2+}-dependent stimulation of PLC may promote cleavage of the sensitizing agent phosphatidylinositol-4,5-bisphosphate (PIP_2) (Liu et al., 2005; Stein et al., 2006; Lishko et al., 2007; Lukacs et al., 2007; Yao and Qin, 2009; Mercado et al., 2010). Although depletion of PIP_2 is thought to play a major role in desensitization (Lukacs et al., 2007; Mercado et al., 2010), artificial depletion of PIP_2 does not completely reproduce the near-full desensitization observed in the presence of calcium (Lukacs et al., 2007).

A third proposed mechanism is the inactivation of TRPV1 via interactions with Ca^{2+}–calmodulin (CaM) (Numazaki et al., 2003; Rosenbaum et al., 2004; Lishko et al., 2007; Grycova et al., 2008). CaM is a ubiquitous and highly conserved 17-kD protein. It comprises two globular domains, the N- and C-lobes, connected by a central flexible linker that allows CaM to assume different conformations (Barbato et al., 1992; Tjandra et al., 1995). Each lobe contains two helix-loop-helix Ca^{2+}-binding motifs known as EF hands and can thus bind four Ca^{2+} ions (Vetter and Leclerc, 2003). Apo–CaM and Ca^{2+}–CaM interact differently with many proteins including ion channels (Gordon-Shaag et al., 2008), making them versatile modulators of various proteins. CaM exhibits diverse mechanisms, sometimes acting through multiple sites, as shown for several TRP channels (Zhu, 2005); its target recognition mechanisms are nearly as promiscuous as its functions (Hoeflich and Ikura, 2002; Yamniuk and Vogel, 2004).

Although TRPV1 does not have a recognizable CaM-binding motif (Rhoads and Friedberg, 1997), at least two CaM-binding sites have been identified in TRPV1 cytosolic domains. In vitro studies demonstrated that Ca^{2+}–CaM binds isolated TRPV1 peptides from the TRPV1-ARD (Rosenbaum et al., 2004). In addition, Ca^{2+}–CaM competes for a shared binding site on TRPV1-ARD with ATP, which sensitizes the channel to capsaicin and prevents tachyphylaxis (Lishko et al., 2007). A second CaM-binding site was localized to a short 35-residue segment in the C terminus of TRPV1 (TRPV1-CT) through in vitro binding assays (Numazaki et al., 2003). Deletion of this segment disrupts desensitization of TRPV1 to repeated stimulation by capsaicin. Furthermore, several mutations to positively charged residues within this region decreased the Ca^{2+}–CaM-binding affinity of TRPV1-CT (Grycova et al., 2008). It is unclear how Ca^{2+}–CaM participates in desensitization of TRPV1 through its putative CaM-binding sites. It has been postulated that Ca^{2+}–CaM may bridge the two sites, leading to a closed channel (Lishko et al., 2007).

Here, we present the first structural view of Ca^{2+}–CaM in complex with the 35-residue CaM-binding peptide from the TRPV1-CT (TRPV1-CT35: residues 767–801). Despite the absence of a classical CaM recognition motif, the complex is supported by hydrophobic anchors and electrostatic interactions similar to well-characterized Ca^{2+}–CaM peptide complexes. Our in vitro binding studies revealed that the C-lobe of Ca^{2+}–CaM is the major determinant of binding to either TRPV1-CT or TRPV1-ARD. We examined whether Ca^{2+}–CaM can bridge contacts between TRPV1-ARD and TRPV1-CT35, but our results do not support such a ternary complex. We used mutations that disrupt Ca^{2+}–CaM binding at either TRPV1-ARD (K155A) or TRPV1-CT (W787A) to show that the W787A TRPV1 mutant is sufficient to disrupt the interaction of Ca^{2+}–CaM with full-length TRPV1, consistent with our in vitro observation that the TRPV1-CT is a high affinity binding site, with $K_d = 5.4 \pm 0.6 \times 10^{-8}$ M. Finally, although the K155A mutation abolished tachyphylaxis, W787A caused slowed and reduced TRPV1 desensitization. In summary, the TRPV1-ARD is crucial for desensitization, although it is unclear whether this is through a direct interaction with CaM, whereas TRPV1-CT is the major CaM interaction site but plays only a minor role in the capsaicin-induced desensitization we measured.

MATERIALS AND METHODS

Expression vectors

The TRPV1-CT regions (759–802, TRPV1-CT44; and 767–801, TRPV1-CT35) were cloned into SacI and EcoRI sites of pMALC2 (New England Biolabs, Inc.) as N-terminal maltose-binding protein (MBP) fusions with a PreScission (GE Healthcare) protease site (LEVLFQGP). CaM C-lobe (residues 76–148) was cloned into NdeI and BamHI sites of pET21a (EMD Millipore). Full-length TRPV1 was expressed from pTracer-CMV2 (Lishko et al., 2007) for electrophysiology or pCDNA3-FLAG for pulldown assays. TRPV1 containing the glycosylation site mutation N604S (Rosenbaum et al., 2002) was cloned into NdeI and NotI sites of pCDNA3-FLAG. pCDNA3-FLAG was generated by ligating a short double-stranded oligonucleotide (5′-GATCACATATGGGATCCGAATTCGTCGACACTAGTGACGTCGCGGCCGCTGATTACAAGGATGACGACGATAAGTGACTCGAG-3′ and 5′-GGCCCTCGAGTCACTTATCGTCGTCATCCTTGTAATCAGCGGCCGCGACGTCACTAGTGTCGACGAATTCGGATCCCATATGT-3′) into the BamHI and NotI sites of pCDNA3 and mutating the NdeI site within the CMV promoter to TATATG. Cysteine mutants of CaM and TRPV1-CT were introduced using QuikChange site-directed mutagenesis (Agilent Technologies) and confirmed by DNA sequencing.

Protein purification

Purification of CaM and TRPV1-ARD was performed as described previously (Drum et al., 2001; Lishko et al., 2007). CaM C-lobe,

CaM_{A15C}, and CaM_{E127C} were purified as CaM. MBP-TRPV1-CT44 or -CT35 was expressed in BL21(DE3) induced at OD_{600} = 0.6 with 100 µM IPTG at 37°C for 2 h. Cells were lysed by sonication in buffer A (20 mM Tris-HCl, pH 7.5, 200 mM NaCl, 0.5 mM PMSF, and 1 mM benzamidine) with 0.1% Triton X-100, 40 µg/ml DNase, 80 µg/ml RNase, and 200 µg/ml lysozyme. The cleared lysate was diluted at 1:1 with buffer A supplemented with 2 mM $CaCl_2$, loaded onto amylose resin (New England Biolabs, Inc.), washed with buffer B (20 mM Tris, pH 7.5, 200 mM NaCl, 1 mM DTT, and 1 mM $CaCl_2$) plus 0.5 mM PMSF, and eluted with buffer B plus 10 mM maltose. To obtain TRPV1-CT44/35, MBP-TRPV1-CT44/35 was concentrated and cleaved with PreScission protease overnight at 4°C. TRPV1-CT44/35 was purified on a Superdex 75 (GE Healthcare) in 20 mM Tris, pH 7.5, 50 mM NaCl, and 1 mM DTT, concentrated, and stored at −80°C. Preparation of MBP-TRPV1-CT35 for binding assays was as above with slight modifications: (a) $CaCl_2$ was excluded from all buffers; (b) 1 mM EDTA was added to lysis buffer; and (c) additional wash with buffer C (20 mM Tris, pH 7.5, 25 mM NaCl, and 1 mM DTT) and 1 mM PMSF was done before elution with buffer C and 10 mM maltose.

To obtain Ca^{2+}-CaM–TRPV1-CT44/35 complex, CaM and excess TRPV1-CT44/35 (1:1.25–2.0 molar ratio) were incubated in 20 mM Tris, pH 7.5, 200 mM NaCl, and 0.15 mM $CaCl_2$. Ca^{2+}-CaM–TRPV1-CT44 complex was isolated on Superdex 75 (GE Healthcare).

Structure determination

Crystals of Ca^{2+}-CaM–TRPV1-CT35 (mixed at a 1.3:1 ratio at ∼8 mg/ml in 20 mM Tris-HCl, pH 7.5, 100 mM NaCl, 1 mM $CaCl_2$, and 1 mM DTT) were grown by vapor diffusion at room temperature against reservoir solution (0.1 M MES, pH 6.0, and 2.2–2.8 M $(NH_4)_2SO_4$), transferred into reservoir plus 25% glycerol, and flash-cooled in liquid nitrogen. Crystals of the two disulfide cross-linked complexes were grown in very similar conditions. Diffraction data, collected at beamlines 24-ID-C and -E (Advanced Photon Source, Argonne National Laboratory) at 0.97949 Å, were processed using HKL2000 (Otwinowski and Minor, 1997). The structure was determined by molecular replacement using CaM coordinates of Protein Data Bank accession number 3DVE (Kim et al., 2008) as a search model. Model building was performed using COOT (Emsley and Cowtan, 2004), and restrained TLS refinement was performed using REFMAC5 (Murshudov et al., 1997). The final wild-type model includes CaM residues 3–148 and TRPV1-CT35 residues 784–798 (deposited in the Protein Data Bank under accession no. 3SUI), with 93% of residues in most favored, 7% in allowed, and none in disallowed regions of the Ramachandran plot. Data and refinement statistics are shown in Table 1 and Table S1.

Binding assays

For CaM-agarose binding of MBP-tagged TRPV1-CT peptide, 60 µg MBP-TRPV1-CT35 in 500 µl of binding buffer (20 mM Tris-HCl, pH 7.5, 100 mM NaCl, 0.1% TWEEN20, and 1 mM DTT) supplemented with either 1 mM EGTA or 1 mM $CaCl_2$ was incubated with preequilibrated CaM-agarose (100 µl of 50% slurry; Sigma-Aldrich) at 4°C for 1 h. Beads were washed three times with 1 ml of the respective binding buffers and resuspended in sample dye plus 5 mM EGTA, and bound protein was analyzed by SDS-PAGE.

For CaM-agarose binding of FLAG-tagged TRPV1, HEK293 cells were transiently transfected with the pCDNA3-FLAG–based vectors using Lipofectamine 2000 (Invitrogen). Cells were harvested in TNE buffer (10 mM Tris-HCl, pH 7.5, 150 mM NaCl, and 1 mM EDTA) 30–40 h after transfection, collected by centrifugation at 2,000 *g*, and lysed in 1 ml TNE buffer supplemented with 1× Complete protease inhibitor (Roche) and 1% IGEPAL (Sigma-Aldrich). The detergent-soluble fraction was divided into two fractions, adding EDTA to 4 mM to one and $CaCl_2$ to 2 mM to the second. CaM-agarose (100 µl of 50% slurry in TNE buffer supplemented with 1× protease inhibitor and either 4 mM EDTA or 2 mM $CaCl_2$) was added. After a 2-h incubation, beads were washed five times with 1 ml of the respective buffers and eluted in 80 µl of 2× SDS sample buffer supplemented with 10 mM EGTA.

Tryptophan fluorescence

Fluorescence experiments were performed using a fluorescence spectrophotometer (Cary Eclipse; Agilent Technologies) at room temperature, in 10 mM Tris-HCl, pH 7.5, and 100 mM KCl, with 1 mM $CaCl_2$ or 5 mM EDTA. Tryptophan excitation was set to 295 nm to minimize contributions of CaM tyrosines to the emission spectra. Emission spectra were recorded from 305 to 400 nm. Excitation and emission bandwidths were set at 5 nm. For intrinsic Trp fluorescence measurements of TRPV1-CT44, 10-mm pathlength cuvettes and a 1-ml volume were used to measure 10 µM TRPV1-CT44 alone or with 10 µM CaM in the presence of $CaCl_2$ or EDTA. For K_d determination, a 5-mm pathlength quartz cuvette (1 ml volume) was used. TRPV1-CT44 at 0.1 µM in 1 ml was titrated with CaM from stocks of 0.04–1 mM, such that the final added volume was <2% of total volume. Fluorescence intensity at 330 nm was monitored, and results from three replicates were analyzed using one site-specific binding nonlinear regression analysis (Prism 5; GraphPad). Nonspecific binding from titrations of TRPV1-CT44 with CaM in EDTA was subtracted from total binding from the same titrations in $CaCl_2$.

Size-exclusion chromatography (SEC) of TRPV1-ARD–CaM interactions

SEC runs were performed as described previously (Lishko et al., 2007). In brief, 60 µM of TRPV1-ARD and 60 µM of CaM or CaM mutants were preincubated in running buffer (20 mM HEPES, pH 7.4, 140 mM NaCl, 1 mM DTT, and 0.16 mM $CaCl_2$) for 30 min on ice, followed by separation on a Superdex 75 column (GE Healthcare) at 4°C.

Disulfide cross-linked Ca^{2+}–CaM/V1-CT35 mutants

Possible disulfide bonds between Ca^{2+}–CaM and TRPV1-CT35 were predicted (CaM_{A15}/V1-$CT35_{N789}$ and CaM_{E127}/V1-$CT35_{R785}$) based on Cβ-Cβ distances using the SSBOND program (Hazes and Dijkstra, 1988). Both pairs were generated by mutagenesis, and all four resulting constructs were purified as above. To test cross-linking, 20 µg CaM_{E127C} or CaM_{A15C} alone or with TRPV1-$CT35_{R785C}$ or TRPV1-$CT35_{N789C}$, respectively, was mixed in 20 mM Tris-HCl, pH 7.5, 100 mM NaCl, and 1 mM $CaCl_2$, and incubated on ice for 20 min. DTT (10 mM final) or $CuSO_4$-1,10 phenanthroline (1–4 mM final) was added and incubated for an additional 20 min. Samples were resolved on 16% T 3% C Tricine SDS-PAGE with 4% T 3% C stacking gel as described previously (Schägger, 2006), in either reducing or nonreducing sample buffers, using running buffer supplemented with 1 mM $CaCl_2$.

For purification of CaM_{E127C}/V1-$CT35_{R785C}$, CaM_{E127C} and TRPV1-$CT35_{R785C}$ were mixed at a 1:1.5 ratio in 20 mM Tris-HCl, pH 7.5, 100 mM NaCl, and 1 mM $CaCl_2$, and 1–4 mM $CuSO_4$-1,10 phenanthroline was added after 20 min, with an additional 20-min incubation on ice. For purification of CaM_{A15C}/V1-$CT35_{N789C}$, CaM_{A15C} and TRPV1-$CT35_{N789C}$ were mixed at a 1:2 ratio in 20 mM Tris-HCl, pH 7.5, 100 mM NaCl, 2 mM $CaCl_2$, 3 mM GSH, and 0.3 mM GSSG and incubated at room temperature overnight. Cross-linked samples were dialyzed in 20 mM Tris-HCl, pH 7.5, 100 mM NaCl, and 1 mM $CaCl_2$ and purified on a Superdex 75 (GE healthcare) column.

Electrophysiology

Whole cell patch-clamping recordings were performed in HEK293 cells transiently transfected using Lipofectamine and PLUS reagent (Invitrogen). Currents were recorded 24–36 h after transfection in voltage-ramp experiments as described previously

(Lishko et al., 2007) or in voltage-clamp experiments at a holding potential of −60 mV. Standard bath solution contained 10 mM HEPES, pH 7.4, 150 mM NaCl, 5 mM KCl, 2 mM $CaCl_2$, 1 mM $MgCl_2$, and 10 mM glucose. Intracellular solution contained 10 mM HEPES-CsOH, pH 7.2, 140 mM Cs-methanesulfonate, 10 mM EGTA, and 2.5 mM NaCl.

Surface biotinylation assay

Transfected HEK293 cells were rinsed twice with ice-cold PBS, pH 8.0, and incubated with 0.5 mg/ml sulfo-NHS-Biotin (Thermo Fisher Scientific) in PBS, pH 8.0, for 30 min at 4°C. Cells were rinsed twice with cold 100 mM glycine in PBS and three times with PBS, lysed in 1 ml of RIPA buffer (50 mM Tris-HCl, pH 7.5, 150 mM NaCl, 1% NP-40, 0.5% sodium deoxycholate, 0.1% SDS, 1 mM EDTA, and 1× protease inhibitor cocktail from Roche), for 1 h at 4°C. Cleared lysates normalized for total protein concentration were incubated with 50 µl of 50% streptavidin-agarose slurry (Sigma-Aldrich) for 1 h at 4°C. The beads were washed three times with RIPA buffer and eluted with 50 µl of 2× SDS sample buffer.

Online supplemental material

Table S1 contains data and refinement statistics for the two cross-linked Ca^{2+}-CaM–TRPV1-CT35 crystal structures. Fig. S1 shows formation of the Ca^{2+}-CaM–TRPV1-CT44 complex by SEC. Fig. S2 shows CaM-agarose pulldown assay results for several TRPV1-CT35 mutants. Fig. S3 shows SEC traces of experiments with rat TRPV1-ARD and CaM mutants. Fig. S4 shows SEC traces probing a possible ternary interaction between TRPV1-ARD, CaM, and TRPV1-CT. Fig. S5 illustrates the crystal structures of the two cross-linked Ca^{2+}-CaM–TRPV1-CT35 complexes. Fig. S6 shows voltage-clamp experiments and cell surface biotinylation of TRPV1 mutants expressed in HEK293 cells. The online supplemental material is available at http://www.jgp.org/cgi/content/full/jgp.201210810/DC1.

RESULTS

High affinity interaction of TRPV1-CT with Ca^{2+}–CaM

A short 35-residue segment (residues 767–801) was identified as a CaM-binding site in TRPV1-CT (Numazaki et al., 2003). In the same study, a longer 44-residue segment (residues 759–802) spanning this site was observed to bind CaM in the absence or presence of Ca^{2+} in a GST pulldown assay. We used SEC to evaluate the interaction of CaM to the 44-residue segment (TRPV1-CT44) and the 35-residue segment (TRPV1-CT35; Fig. 1 A). TRPV1-CT44 and TRPV1-CT35 undergo a large shift in elution volume when mixed with CaM in the presence of Ca^{2+}, confirming that a complex is formed (Figs. 1 B and S1; data shown for TRPV1-CT44).

To obtain a quantitative measurement of Ca^{2+}–CaM binding to TRPV1-CT, we took advantage of the intrinsic tryptophan present in TRPV1-CT peptides to monitor its binding to Ca^{2+}–CaM. We used TRPV1-CT44, which is more readily produced in large quantities and high purity than TRPV1-CT35. The fluorescence emission peak of tryptophan in TRPV1-CT44 is 354 nm (Fig. 1 C). In the presence of CaM in $CaCl_2$ but not EDTA, the fluorescence emission peak blue-shifted to 330 nm and fluorescence intensity was enhanced, consistent with a tryptophan residue in a hydrophobic environment (Gomes et al., 2000; Weljie and Vogel, 2000).

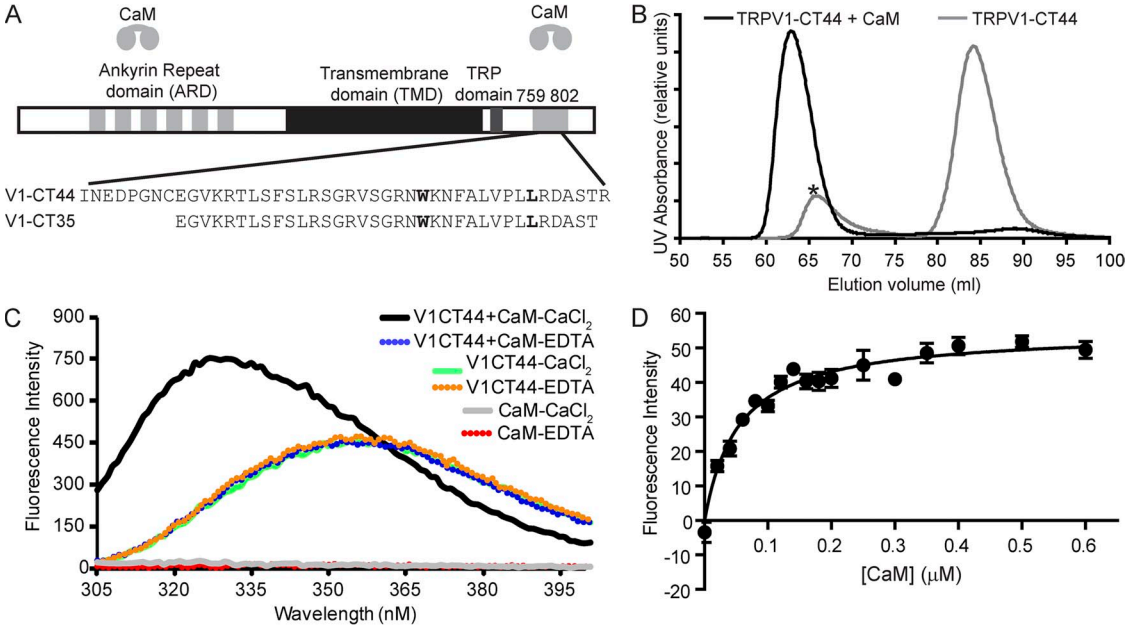

Figure 1. TRPV1-CT CaM-binding site. (A) Schematic diagram showing the domain organization of TRPV1. CaM and putative CaM-binding sites are shaded in light gray. (B) SEC elution profile of TRPV1-CT44 alone or in complex with Ca^{2+}–CaM. Shown are representative traces of a TRPV1-CT44 preparation (gray) after cleavage of an MBP tag (*) and Ca^{2+}-CaM–TRPV1-CT44 complex (black). (C) Tryptophan fluorescence emission spectra of 10 µM TRPV1-CT44 (residues 759–802) alone or incubated with equimolar amounts of CaM in the presence of $CaCl_2$ or EDTA, excited at 295 nm. (D) Titration of 0.1 µM TRPV1-CT44 with CaM from 0.01 to 1 µM in the presence of $CaCl_2$. Tryptophan fluorescence emission at 330 nm was plotted against CaM concentration. Data were obtained in triplicate and analyzed using one site-specific binding nonlinear regression analysis (Prism 5; GraphPad). Line shows the best fit to the data ($K_d = 5.4 \pm 0.6 \times 10^{-8}$ M).

Our results further confirm that TRPV1-CT interacts with CaM in a Ca^{2+}-dependent manner. In a titration experiment, we measured that TRPV1-CT44 interacts with Ca^{2+}–CaM in a 1:1 ratio with high affinity, $K_d = 5.4 \pm 0.6 \times 10^{-8}$ M (Fig. 1 D), comparable to other Ca^{2+}–CaM-binding targets (Crivici and Ikura, 1995). Our results establish the distal TRPV1-CT region as a high affinity binding site for Ca^{2+}–CaM.

Overall structure of Ca^{2+}-CaM–TRPV1-CT peptide complex

TRPV1 does not have a classical CaM recognition motif (Rhoads and Friedberg, 1997). To better understand the Ca^{2+}–CaM interaction with TRPV1-CT, we determined the crystal structure of Ca^{2+}–CaM in complex with TRPV1-CT35 (residues 767–801) to 1.95-Å resolution (Fig. 2 A and Table 1). The asymmetric unit contains a 1:1 Ca^{2+}-CaM–TRPV1-CT35 complex. Residues 784–798 of TRPV1-CT were observed in the structure (Fig. 2 A), with the electron density well defined for residues 785–797 (Fig. 2, B and C). As expected, four Ca^{2+} ions are observed in the structure, with two in each CaM lobe. TRPV1-CT35 adopts an elongated structure, with a helix (residues 787–796) flanked by two extended peptide regions (Fig. 2 A). The helical peptide is clasped by both Ca^{2+}–CaM lobes in an antiparallel orientation, with its N terminus interacting with the Ca^{2+}–CaM C-lobe and its C terminus bound to the N-lobe. This overall Ca^{2+}-CaM–TRPV1-CT35 structure is similar to several canonical Ca^{2+}–CaM peptide complexes (Yamniuk and Vogel, 2004), including those of smooth muscle light chain kinase (Meador et al., 1992), Ca^{2+}–CaM-dependent kinase kinase (CaMKK) (Kurokawa et al., 2001), and endothelial nitric oxide synthase (Aoyagi et al., 2003).

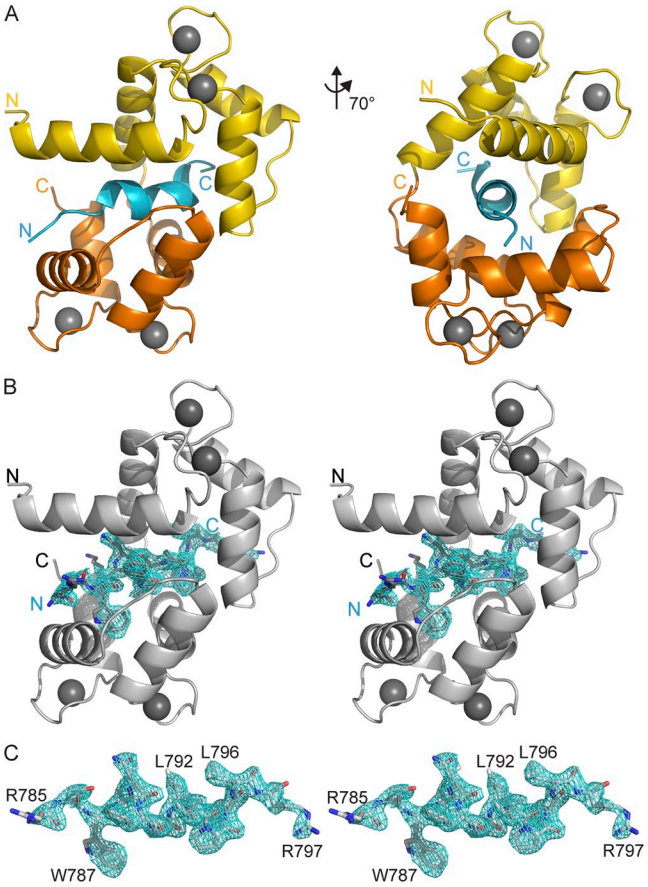

Figure 2. Structure of a TRPV1-CT peptide in complex with Ca^{2+}–CaM. (A) Ribbon diagrams of TRPV1-CT35 (cyan) bound to Ca^{2+}–CaM, shown in two different orientations; the view on the right is rotated 70° around the vertical axis with respect to the one on the left. The CaM N-lobes and C-lobes are yellow and orange, respectively, and the calcium ions are gray. (B) Stereoview of TRPV1-CT35 (stick representation; residues 785–797) bound to Ca^{2+}–CaM (gray ribbons with dark gray Ca^{2+} ion spheres). The $2F_o$–F_c electron density map corresponding to TRPV1-CT35 is shown in cyan, contoured at 1.0 σ. (C) Stereoview of TRPV1-CT35 in stick representation with the corresponding $2F_o$–F_c electron density map contoured at 1.0 σ (cyan). Several key residues are labeled.

TRPV1-CT target recognition and binding by Ca^{2+}–CaM

In canonical Ca^{2+}–CaM peptide complexes, the peptide is anchored through interactions of two large hydrophobic residues to hydrophobic pockets, one on each Ca^{2+}–CaM lobe (Fig. 3 A). The relative sequence position of the anchor residues defines the binding mode of Ca^{2+}-CaM–peptide complexes. TRPV1-CT35 is indeed anchored to hydrophobic pockets on the C- and N-lobes of Ca^{2+}–CaM through hydrophobic anchor residues W787 and L796 at the C- and N-lobe, respectively (Fig. 3 B).

TABLE 1

Data collection and refinement statistics for the Ca^{2+}-CaM–TRPV1-CT35 crystal structure

Data collection	
Space group	$P6_122$
Unit cell dimensions (*a*, *b*, *c*; Å)	41.68, 41.68, 341.53
Resolution (Å)	50.0–1.95 (1.98–1.95)
R_{sym}	5.2 (46.9)
$I/\sigma I$	26.4 (2.5)
Completeness (%)	98.0 (91.2)
Redundancy	5.4 (3.9)
Refinement	
Resolution (Å)	36.10–1.95
No. reflections	13,172
R_{work}/R_{free}	19.2/24.9
No. atoms	1,438
No. protein atoms	1,339
No. ligand atoms	4 (Ca^{2+}) + 5 (SO_4^{2-})
No. water atoms	90
Average protein *B*-factors	42.72
Average ligand/ion *B*-factors	61.38
Average water *B*-factors	27.30
RMS deviations of bond lengths (Å)	0.0176
RMS deviations of bond angles (°)	1.5601

TRPV1-CT35 therefore has a 1–10 motif like that of CaM-dependent kinase II (Meador et al., 1993).

The N-terminal anchor, W787, forms extensive hydrophobic contacts with surrounding residues F92, L105, M124, and M144, lining a deep hydrophobic pocket in the Ca^{2+}–CaM C-lobe (Fig. 3 B). These four residues form the $FLMM_C$ tetrad, which is conserved in its interaction with its target anchor, whereas the $FLMM_N$ tetrad in the N-lobe (F19, L32, M51, and M71) is more variable (Ataman et al., 2007). The TRPV1-CT anchor, L796, contacts F19, M51, and M71 from the $FLMM_N$ tetrad (Fig. 3 B). In addition to the anchor residues, other hydrophobic residues along the TRPV1-CT35 α helix, namely F790, A791, L792, V793, P794, and L795, also form extensive hydrophobic contacts with both the N- and C-lobes of Ca^{2+}–CaM (Fig. 3 D).

Although hydrophobic residues are major determinants of CaM interactions, basic residues mediate electrostatic contacts with the highly acidic surface of CaM and can drive the orientation of the bound CaM target (Osawa et al., 1999; Yamniuk and Vogel, 2004). Antiparallel Ca^{2+}–CaM targets have positive residues near the N-terminal anchor, whereas in the case of parallel Ca^{2+}–CaM targets, basic residues flank the CT anchor (Fig. 3 A). This preferential distribution of basic residues around one anchor or the other in an antiparallel or parallel target can be understood from examining the complementary electrostatic surfaces on Ca^{2+}–CaM, which are important in determining the orientation of the bound peptide (Osawa et al., 1999). In our structure, basic residues R785 and K788 flank the N-terminal hydrophobic anchor W787 near the highly electronegative opening in the Ca^{2+}–CaM structure, whereas the single CT basic residue, R797, is oriented toward the less electronegative opening (Fig. 4 A). In summary, although no canonical CaM-binding sequence is found in the TRPV1-CT,

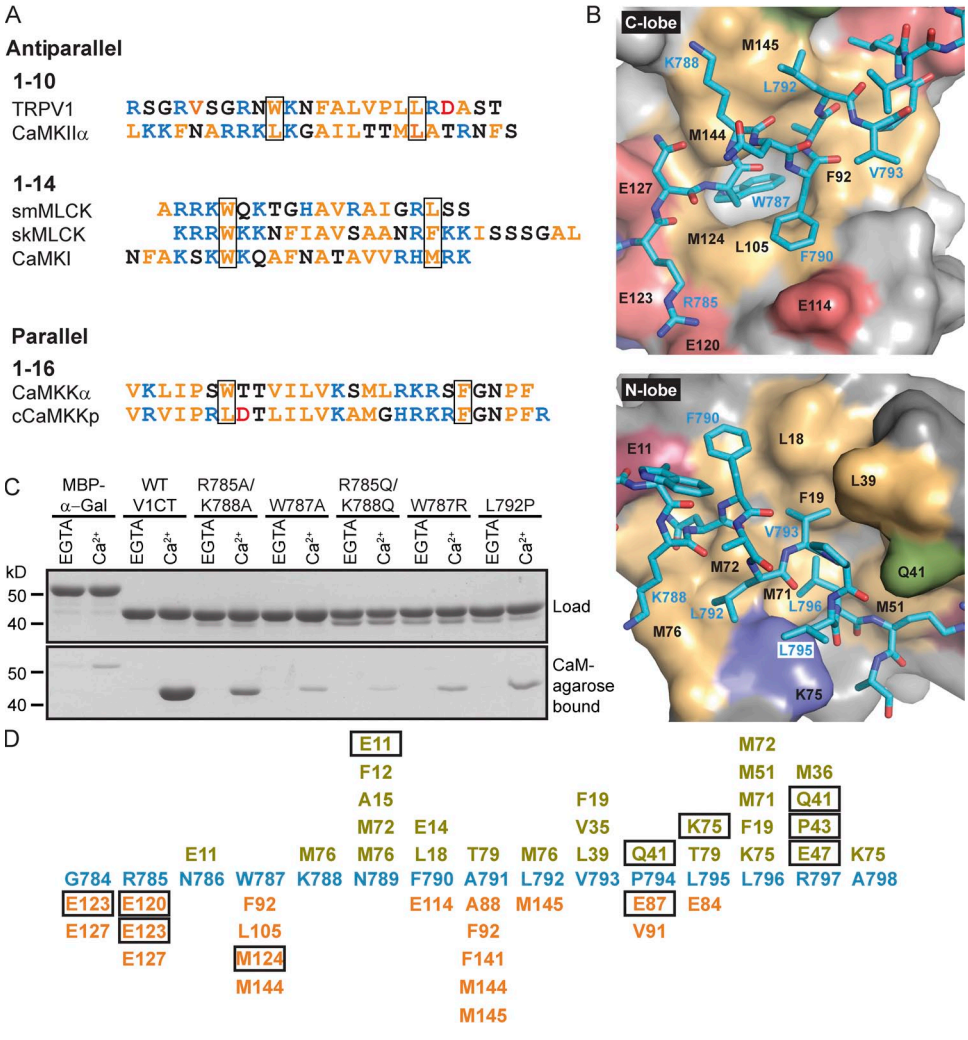

Figure 3. The Ca^{2+}-CaM–TRPV1-CT interface. (A) Aligned sequences of Ca^{2+}–CaM-binding peptides with antiparallel 1–10 motifs (TRPV1-CT and CaMKIIa; Meador et al., 1993) and 1–14 motifs (smooth muscle light chain kinase [Meador et al., 1992], skMLCK [Ikura et al., 1992], and CaMKI [Clapperton et al., 2002]), and parallel 1–16 motifs (CaMKKα [Osawa et al., 1999] and cCAMKKp [Kurokawa et al., 2001]). Residues are colored as follows: blue, positively charged; red, negatively charged; orange, hydrophobic. Hydrophobic anchors are boxed in black. (B) Lobe-specific interactions, featuring hydrophobic pockets on CaM, with the CaM C-lobes and N-lobes shown in surface representation. The views of the C-lobes and N-lobes are related to Fig. 2 A by rotations of +80° and −100° around the horizontal axis, respectively. CaM residues that contact TRPV1-CT35 (interatomic distances of ≤4.2 Å) are colored according to their side-chain properties (orange, hydrophobic; blue, positively charged; red, negatively charged; green, polar), and selected ones are labeled in black. Selected TRPV1 residues are labeled in cyan. (C) CaM-agarose pulldowns of MBP-fused TRPV1-CT35 peptides (residues 767–801). A Coomassie-stained gel of pulldowns in the absence (EGTA) or presence (Ca^{2+}) of calcium is shown as a representative result of three independent experiments. An MBP–α-Gal protein construct, expressed from the unmodified vector, was used as a negative control. (D) Sequence map of CaM residues in contact with TRPV1-CT35 (interatomic distances of ≤4.2 Å). CaM N-lobe, C-lobe, and TRPV1-CT35 residues are mustard, orange, and cyan, respectively. Interacting CaM residues making at least one polar contact are boxed.

residues 785–797 of TRPV1 interact with Ca^{2+}–CaM using hydrophobic anchors and electrostatic interactions similar to those found in well-characterized Ca^{2+}–CaM-target complexes.

Unique features of the Ca^{2+}-CaM–TRPV1-CT35 peptide complex

The Ca^{2+}-CaM–TRPV1-CT35 complex exhibits several unique features. The first is the structure of the TRPV1-CT peptide, which consists of a short 10-residue helix flanked by two extended peptide regions (Fig. 2 A), unlike classical Ca^{2+}–CaM targets that assume longer α-helical structures (Rhoads and Friedberg, 1997; Yamniuk and Vogel, 2004). Sets of available structures comprising eight parallel and 31 antiparallel Ca^{2+}-CaM–peptide structures had Ca^{2+}–CaM-interacting helices averaging 18.4 and 18.8 residues in length, respectively. Within these sets, only two other Ca^{2+}–CaM targets have short helices similar to TRPV1: the Ca^{2+}–CaM-binding domain of myristoylated alanine-rich C kinase substrate (MARCKS; Protein Data Bank accession no. 1IWQ; eight-residue helix) (Yamauchi et al., 2003) and the Ca^{2+}-CaMKK (Protein Data Bank accession no. 1CKK; 11-residue helix) (Osawa et al., 1999). The MARCKS and TRPV1-CT peptides share the same antiparallel orientation with respect to Ca^{2+}–CaM, whereas the CaMKK peptide has a parallel orientation. The conformation of Ca^{2+}–CaM in the TRPV1-CT complex is very similar to that of the MARCKS peptide-bound Ca^{2+}–CaM (root-mean-square deviation [RMSD] = 0.646 Å). However, in contrast to the 1–10 binding mode of TRPV1-CT35, MARCKS has no hydrophobic anchor bound to the Ca^{2+}–CaM N-lobe hydrophobic pocket. This highlights not only the conformational flexibility of Ca^{2+}–CaM to recognize its different targets but also the variability of CaM targets that can fit into the same Ca^{2+}–CaM scaffold.

A second feature unique to TRPV1-CT is that the two hydrophobic anchors are at the boundaries of the α-helical region (Fig. 4 B), whereas those of classical Ca^{2+}–CaM targets are present within the α helix. Out of the nearly 40 available Ca^{2+}-CaM–peptide complex structures that we analyzed, the only Ca^{2+}–CaM target that also carries a nonhelical hydrophobic anchor is the CaMKK peptide. However, the binding modes of CaMKK and TRPV1-CT are different in all other aspects. The CaMKK peptide exhibits a parallel 1–16 binding mode, with an N-terminal tryptophan hydrophobic anchor on the α helix and its CT anchor, a phenylalanine residue, on the extended CT region (Osawa et al., 1999). In summary, the structure of the Ca^{2+}-CaM–TRPV1-CT complex revealed yet another variation of Ca^{2+}–CaM target recognition motifs, with a 1–10 antiparallel binding mode in which both hydrophobic anchors bound the peptide helix.

Both hydrophobic and positively charged residues are important determinants of binding

Interestingly, the Ca^{2+}–CaM-binding site observed in our crystal structure overlaps a previously proposed PIP_2-binding site required for PIP_2-mediated inhibition of TRPV1 activity (Prescott and Julius, 2003), although this study's conclusions are controversial (see Discussion). In the study, substitution of several basic residues by neutral polar residues resulted in increased sensitivity of TRPV1 to both chemical and heat stimuli. This phenotype was interpreted as a relief of inhibitory PIP_2 interactions with TRPV1. In particular, the R785Q/K788Q substitution pair increased TRPV1 sensitivity to heat by shifting the temperature threshold of activation to lower temperatures. Incidentally, R785 and K788 are the two basic residues that flank the hydrophobic tryptophan anchor in our Ca^{2+}–CaM-binding site (Fig. 3 A). To examine whether the region observed in our structure represents bona fide determinants for Ca^{2+}–CaM binding in solution, we mutated several key residues in an MBP-fused TRPV1-CT35 and examined interactions with Ca^{2+}–CaM using a CaM-agarose pulldown assay. Tryptophan is often found in protein interface hot

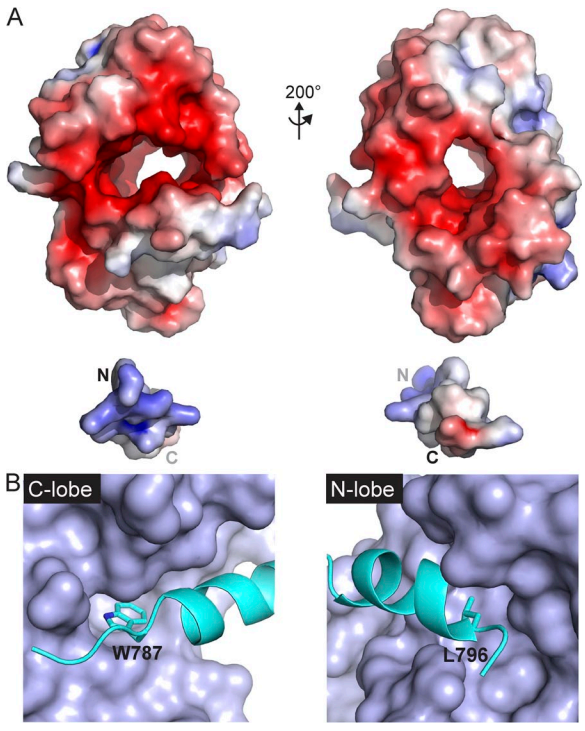

Figure 4. Electrostatic surface potential of Ca^{2+}–CaM and TRPV1-CT peptide. (A) Surface of Ca^{2+}–CaM (top) viewed from N- (left) and CT (right) face of equivalently positioned TRPV1-CT peptide (bottom). The molecular surface is colored according to the electrostatic potential from red (−6 kT/e) to blue (6 kT/e). Electrostatic potential surfaces were generated in PyMOL using APBS (Baker et al., 2001). (B) Cartoon representation of TRPV1-CT peptide against surface representation of binding pocket, showing the hydrophobic anchors: W787 (left) and L796 (right) positioned at the TRPV1-CT helix N and C termini, respectively.

spots responsible for the bulk of binding energy (Bogan and Thorn, 1998), and as anticipated, substitution of the hydrophobic anchor W787 with alanine caused a severe disruption of Ca^{2+}–CaM binding, underscoring the importance of the tryptophan anchor in mediating hydrophobic interactions with Ca^{2+}–CaM (Fig. 3 C). Alanine substitutions at the R785/K788 pair also impaired Ca^{2+}–CaM binding, indicating that these basic residues are likewise crucial for interaction with Ca^{2+}–CaM (Fig. 3 C), consistent with a previously published study (Grycova et al., 2008). Charge-neutralizing R785Q/K788Q substitutions, which were previously shown to potentiate TRPV1 activity (Prescott and Julius, 2003), also impair binding to Ca^{2+}–CaM (Fig. 3 C).

A separate study aimed at identifying active or hypersensitive TRPV1 mutants using a toxicity-based screen (Myers et al., 2008) identified several mutations that fell within our Ca^{2+}–CaM-binding site: W787R, L792P, and L796P. To determine whether these mutations alter Ca^{2+}–CaM binding, we studied the interaction of these mutants using our CaM-agarose pulldown assay. As with W787A, W787R severely disrupted Ca^{2+}–CaM binding (Fig. 3 C). Although mutation of the L796 CT anchor to proline did not significantly disrupt binding of TRPV1-CT35 to Ca^{2+}–CaM in our pulldown assay (Fig. S2), the L792P substitution severely disrupted Ca^{2+}–CaM binding (Fig. 3 C). A proline substitution at L792, which is situated in the middle of the TRPV1-CT35 helix in the Ca^{2+}–CaM-bound structure, would break the helical conformation of the peptide and thus likely displace other necessary Ca^{2+}–CaM interacting groups. In contrast, the L796P substitution is located at the CT end of the helix, providing a likely explanation as to why this mutation is tolerated. Our binding assay agrees well with the observed Ca^{2+}-CaM–TRPV1-CT structural features.

To examine whether phosphorylation of S800, which potentiates TRPV1 (Bhave et al., 2003), interferes with Ca^{2+}–CaM binding, we mutated S800 to either an aspartic acid or glutamic acid to mimic a phosphorylation state. Neither S800D nor S800E interfered with Ca^{2+}–CaM binding (Fig. S3). This result is consistent with our structural data, as S800 lies outside the region observed in our structure (Fig. 3 D) and suggests that disruption of Ca^{2+}–CaM binding is not the cause of the observed phosphorylation-induced potentiation in TRPV1.

Collectively, our mutagenesis results confirmed that TRPV1-CT35 interacts extensively with Ca^{2+}–CaM through both hydrophobic and electrostatic interactions (Fig. 3 D).

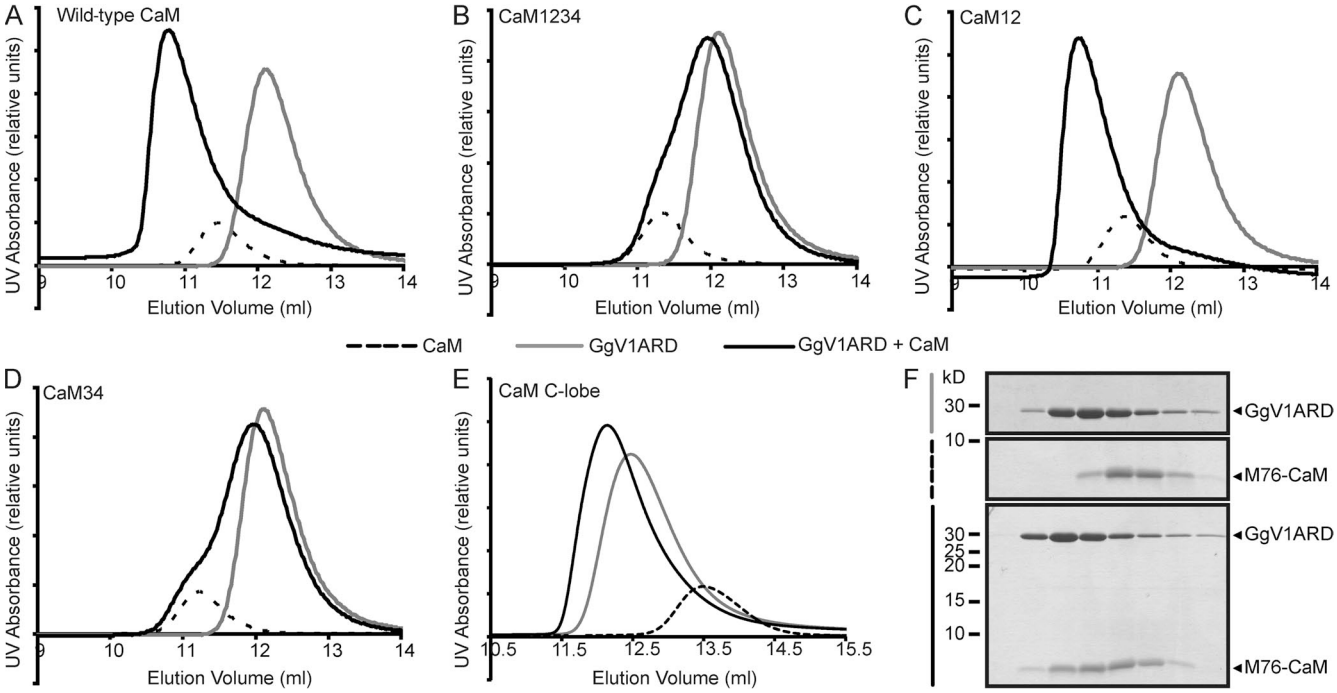

Figure 5. The C-lobe of Ca^{2+}–CaM is necessary and sufficient to interact with chicken TRPV1-ARD. (A–E) SEC elution profiles of chicken (*Gallus gallus*) TRPV1-ARD (GgV1ARD) mixed with various CaM mutants. A physical interaction was observed in the presence of 2 mM Ca^{2+} for wild-type CaM, CaM12, and CaM C-lobe, as indicated by a left-shift of the peak for the mixed proteins (60 µM GgV1ARD and 60 µM CaM; black) compared with elution volumes of the individual proteins (gray, GgV1ARD; dashed black, CaM). Shown are representative traces from two repeats. Wild-type CaM was used in A, followed by CaM mutated at all four Ca^{2+} sites (B, CaM1234), the two N-lobe Ca^{2+} sites (C, CaM12), or the two C-lobe Ca^{2+} sites (D, CaM34). (E) The isolated C-lobe of CaM (residues 76–148) interacts with chicken TRPV1-ARD by SEC. (F) Coomassie-stained gels from SEC runs in E. The lanes from left to right are fractions of increasing elution volume, from 10.5 to 15.5 ml.

Notably, mutation of the N-terminal tryptophan anchor alone is sufficient to severely diminish Ca^{2+}–CaM interaction, suggesting that the C-lobe of Ca^{2+}–CaM dominates the interactions with TRPV1-CT35.

CaM C-lobe alone is sufficient to interact with TRPV1-ARD

The interactions of Ca^{2+}–CaM with both TRPV1-ARD and TRPV1-CT are Ca^{2+} dependent and both regions have been implicated in TRPV1 desensitization, suggesting that both sites may work in concert. One hypothesis is that Ca^{2+}–CaM bridges an interaction between the TRPV1-ARD and TRPV1-CT, leading to a closed channel (Lishko et al., 2007). CaM forms an analogous ternary complex in SK channels, for example, where CaM mediates dimerization of two channel subunits through binding of its N- and C-lobe to two different subunits (Schumacher et al., 2001). Having determined that the C-lobe dominates the TRPV1-CT35 interaction, we asked whether the TRPV1-ARD is similarly dominated by a specific CaM lobe.

We have been unable to measure the affinity of TRPV1-ARD for Ca^{2+}–CaM because of technical difficulties with protein stability under various assay conditions, or to cocrystallize a Ca^{2+}-CaM–TRPV1-ARD complex to determine its structure. Instead, we tested which CaM lobe principally drives the Ca^{2+}-dependent interaction with TRPV1-ARD by using SEC to compare the impact of mutations at the CaM Ca^{2+}-binding sites on the interaction. CaM1, CaM2, CaM3, and CaM4 were mutated at the first (D21A), second (D57A), third (D94A), or fourth (D130A) Ca^{2+}-binding site, respectively. Rat TRPV1-ARD no longer interacted with any of the single-site CaM mutants (Fig. S3). However, rat TRPV1-ARD exhibits only a small shift by SEC when mixed with Ca^{2+}–CaM, perhaps because of a weak interaction that is highly susceptible to perturbations. Slight differences in affinities for the distinct CaM mutants would be missed if any perturbation caused a loss of detectable binding. Therefore, we also tested interactions between the CaM mutants and chicken TRPV1-ARD, which in SEC experiments has a robust shift with wild-type Ca^{2+}–CaM (Fig. 5 A). Chicken TRPV1-ARD showed no interaction with CaM1234, which has all four Ca^{2+}-binding sites mutated (Fig. 5 B), demonstrating that the interaction with CaM is Ca^{2+} dependent. Chicken TRPV1-ARD retained the ability to interact with CaM12 but not CaM34 (Fig. 5, C and D), pointing to the importance of Ca^{2+}–CaM C-lobe in interacting with TRPV1-ARD. Using a truncated CaM (residues 76–148), we further showed that the isolated Ca^{2+}–CaM C-lobe can bind TRPV1-ARD (Fig. 5 E). Although chicken and rat TRPV1-ARD may interact differently with Ca^{2+}–CaM, their close homology (69.5% identity and 82.0% similarity) suggests that they likely share a common binding mode (Phelps et al., 2007). Thus, our results suggest that the Ca^{2+}–CaM C-lobe is crucial for binding to TRPV1-ARD.

The Ca^{2+}-CaM–TRPV1-CT35 complex does not interact with TRPV1-ARD

Although the Ca^{2+}–CaM C-lobe appears to dominate the interactions of both TRPV1-CT and TRPV1-ARD, it remained to be determined whether we could observe a ternary complex between TRPV1-ARD, a TRPV1-CT peptide, and Ca^{2+}–CaM. Using SEC, a shift of the rat TRPV1-ARD peak was observed in the presence of isolated Ca^{2+}-CaM–TRPV1-CT44 complex (Fig. S4). However, we could not unambiguously ascertain whether the observed TRPV1-ARD shift was caused by its interaction with a Ca^{2+}-CaM–TRPV1-CT peptide complex or with Ca^{2+}–CaM alone because of overlapping elution profiles of Ca^{2+}–CaM and the Ca^{2+}-CaM–TRPV1-CT44 complex. To resolve this problem, we introduced cysteine pairs to form disulfide cross-links between Ca^{2+}–CaM and TRPV1-CT35. Any SEC shift of TRPV1-ARD in the presence of cross-linked Ca^{2+}-CaM–TRPV1-CT35 could thereby be attributed to the binding of TRPV1-ARD to a Ca^{2+}-CaM–TRPV1-CT peptide complex.

Two cysteine pairs were engineered based on predicted optimal disulfide bond sites using SSBOND (Hazes and Dijkstra, 1988): TRPV1-CT35 N789C cross-links to A15C in the N-lobe of Ca^{2+}–CaM, and TRPV1-CT35 R785C cross-links to E127C in the Ca^{2+}–CaM C-lobe (Fig. 6 A). Both sets of mutants display a Ca^{2+}-dependent interaction similar to wild-type Ca^{2+}–CaM and TRPV1-CT35, as shown in native gel (Fig. 6 B). Although the E127C–R785C pair cross-linked more efficiently under our original conditions (Fig. 6 C), we were able to isolate both cross-linked complexes with good purity (see Materials and methods). Both cross-linked complexes crystallized under very similar conditions and in the same space group as the wild-type complex, and we determined the Ca^{2+}-CaM_{E127C}–$TRPV1\text{-}CT35_{R785C}$ structure to 2.4-Å resolution, and the Ca^{2+}-CaM_{A15C}–$TRPV1\text{-}CT35_{N789C}$ to 2.1-Å resolution. Both structures exhibited only minimal local conformational variations (Fig. S5). Thus, the introduced cross-links in the Ca^{2+}-CaM–TRPV1-CT peptide complex did not perturb the interactions observed in our original structure.

We then used SEC to investigate whether the cross-linked complexes interact with rat TRPV1-ARD. Neither TRPV1-ARD nor the cross-linked complexes showed a shift in elution volume when incubated together (Fig. 6 D); therefore, the SEC profiles showed no evidence of interaction between TRPV1-ARD and either cross-linked complex. Although we cannot rule out the possibility that cross-linking may interfere with possible conformational requirements for interaction with the TRPV1-ARD, the fact that neither Ca^{2+}-CaM_{E127C}–$TRPV1\text{-}CT35_{R785C}$ nor Ca^{2+}-CaM_{A15C}–$TRPV1\text{-}CT35_{N789C}$ interacted with TRPV1-ARD makes it unlikely that the cross-link itself prevented the interaction. Our results therefore indicate that TRPV1-ARD and TRPV1-CT do not form a ternary complex with Ca^{2+}–CaM under the conditions we tested.

TRPV1-CT is the major determinant for Ca^{2+}–CaM binding

Although both the isolated TRPV1-ARD and TRPV1-CT were shown to interact with Ca^{2+}–CaM in solution, it is unclear how these two sites contribute to Ca^{2+}–CaM binding in full-length TRPV1. To test this, we introduced mutations K155A or W787A, which were shown to abolish Ca^{2+}–CaM binding to TRPV1-ARD (Lishko et al., 2007) and TRPV1-CT (this study), respectively, and determined whether the resulting TRPV1 mutants can still bind Ca^{2+}–CaM using a CaM-agarose pulldown assay. Wild-type TRPV1 expressed from HEK293 cells binds CaM in a Ca^{2+}-dependent manner (Fig. 7 A). K155A did not affect binding of TRPV1 to Ca^{2+}–CaM, whereas W787A severely disrupted binding to Ca^{2+}–CaM, suggesting that the TRPV1-CT alone is sufficient for binding to Ca^{2+}–CaM. Our results support TRPV1-CT as a high affinity Ca^{2+}–CaM-binding site in full-length TRPV1.

Distinct roles of TRPV1-ARD and TRPV1-CT in TRPV1 desensitization

Disruption of Ca^{2+}–CaM binding to TRPV1-ARD was shown to diminish the Ca^{2+}-dependent desensitization of TRPV1 to repeated capsaicin stimulations in whole cell patch-clamp electrophysiology experiments (Lishko et al., 2007). To examine the functional role of the high affinity TRPV1-CT Ca^{2+}–CaM-binding site, we introduced mutations that abolish Ca^{2+}–CaM binding to either TRPV1-ARD (K155A), TRPV1-CT (W787A), or both TRPV1-ARD and TRPV1-CT (K155A/W787A) and compared the capsaicin-evoked currents in HEK293 cells. We measured the maximal current amplitude evoked by each successive pulse of capsaicin using the whole cell patch-clamp technique in voltage ramps (Fig. 8) or at a holding potential of −60 mV (Fig. S6). As expected, repeated applications of capsaicin resulted in strong tachyphylaxis of wild-type TRPV1 currents,

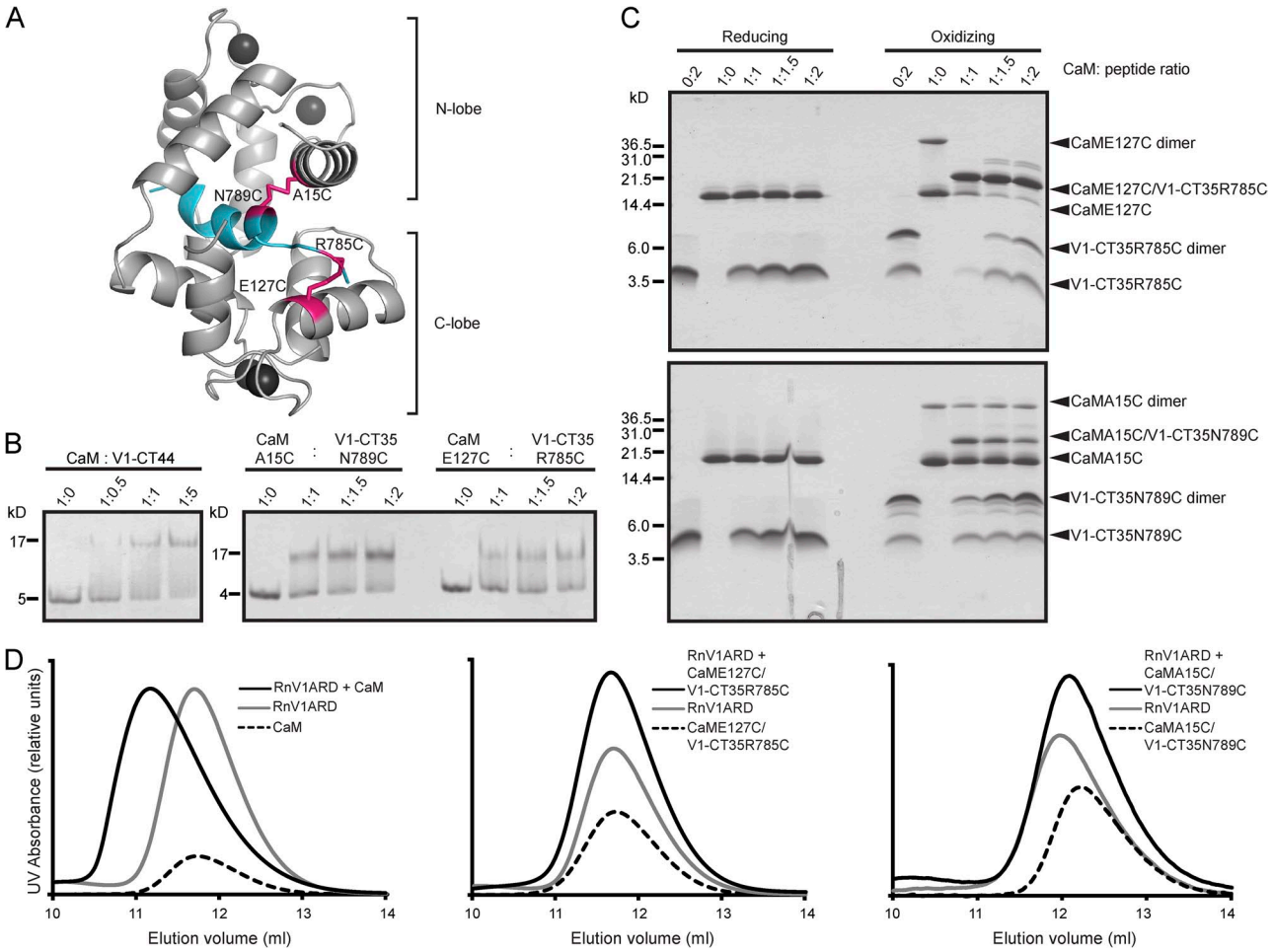

Figure 6. Disulfide-cross-linked Ca^{2+}-CaM–TRPV1-CT35 complexes do not interact with TRPV1-ARD. (A) Ribbon diagram of TRPV1-CT35 (cyan) bound to Ca^{2+}–CaM (gray) with modeled disulfide bonds (pink) based on predictions using SSBOND (Hazes and Dijkstra, 1988). (B) Native-PAGE of CaM or CaM cysteine mutants alone or in the presence of increasing molar ratio of respective TRPV1-CT or TRPV1-CT mutant. (C) Tricine–SDS-PAGE of CaM and TRPV1-CT35 cysteine mutants under reducing or oxidizing conditions. (D) 60 µM of purified rat TRPV1-ARD (RnARD) was mixed with 60 µM CaM (left), 60 µM of the cross-linked complex CaM_{E127C}–$V1\text{-}CT35_{R785C}$ (middle), or 60 µM CaM_{A15C}–$V1\text{-}CT35_{N789C}$ (right) in the presence of $CaCl_2$ and separated using SEC.

observed as decreased inward currents (Fig. 8 A, black trace). K155A showed little tachyphylaxis and slower activation kinetics as reported previously (Lishko et al., 2007). The slower activation kinetics of K155A is not caused by altered surface expression (Fig. S6) and is therefore an inherent quality of the mutant. Although the slower activation kinetics could suggest a constitutively desensitized phenotype, the steady-state inward currents of K155A are larger than those of wild type (Fig. 8 C). Furthermore, it has been reported that desensitization reduces the sensitivity of TRPV1 to capsaicin (Yao and Qin, 2009), whereas we previously determined that the K155A mutant displays normal capsaicin sensitivity (Lishko et al., 2007).

In contrast, the W787A mutant showed desensitization albeit with slower kinetics and significantly higher residual currents in subsequent capsaicin application compared with wild-type TRPV1. As most tachyphylaxis occurs between the first and second application (Mohapatra et al., 2003), we compared the mean maximal current amplitude at −80 mV of the second application to that of the first application. Wild-type TRPV1-expressing cells only retained 2.3 ± 0.4% of their maximal current at the second application, whereas W787A-expressing cells retained 14.4 ± 3.2% (n = 8 and P = 0.006). Our results with the W787A mutation are similar to those obtained when the TRPV1-CT35 region is deleted in full-length TRPV1 (Numazaki et al., 2003), showing that TRPV1-CT is indeed involved in the fast component of TRPV1 desensitization. Disruption of both Ca^{2+}–CaM-binding sites (K155A/W787A) led to capsaicin-induced currents similar to the K155A mutation. In summary, the stronger phenotype elicited by K155A suggests a major role for TRPV1-ARD in TRPV1 desensitization, whereas the more subtle W787A phenotype suggests that TRPV1-CT plays a minor role in capsaicin-induced desensitization but may be involved in other responses not discernible under our experimental conditions.

DISCUSSION

Here, we present the structure of Ca^{2+}–CaM bound to a short 35-residue TRPV1-CT region (TRPV1-CT35), one of two identified Ca^{2+}–CaM-binding sites in TRPV1. The second Ca^{2+}–CaM-binding site was previously identified in TRPV1-ARD (Rosenbaum et al., 2004), where Ca^{2+}–CaM competes with a TRPV1 sensitizer, ATP, for binding (Lishko et al., 2007). Our affinity measurements indicate that TRPV1-CT represents a high affinity binding site for Ca^{2+}–CaM ($K_d = 5.4 \pm 0.6 \times 10^{-8}$ M). Although we could not measure the affinity of TRPV1-ARD for Ca^{2+}–CaM because of technical difficulties, our SEC experiments suggest that the affinity is likely significantly lower than that of the TRPV1-CT. Consistently, a mutation that abolished Ca^{2+}–CaM binding to TRPV1-CT (W787A), but not a corresponding one in TRPV1-ARD (K155A), severely disrupted binding to Ca^{2+}–CaM in full-length TRPV1. The W787A mutation was sufficient to slow and reduce TRPV1 desensitization, consistent with a 35–amino acid deletion mutant that also exhibited reduced Ca^{2+}-dependent desensitization of TRPV1 (Numazaki et al., 2003).

The interaction of Ca^{2+}–CaM with TRPV1-CT35 is similar to that observed in canonical Ca^{2+}–CaM/target complexes. The bound peptide adopts an α-helical conformation and binds Ca^{2+}–CaM in an antiparallel manner through two hydrophobic anchors, W787 and L796, corresponding to a 1–10 binding motif. Sequence alignment of the TRPV1-CT CaM-binding site identified in the rat TRPV1 sequence with TRPV1 from other species shows that this site is conserved (Fig. 7 B), suggesting a conserved function.

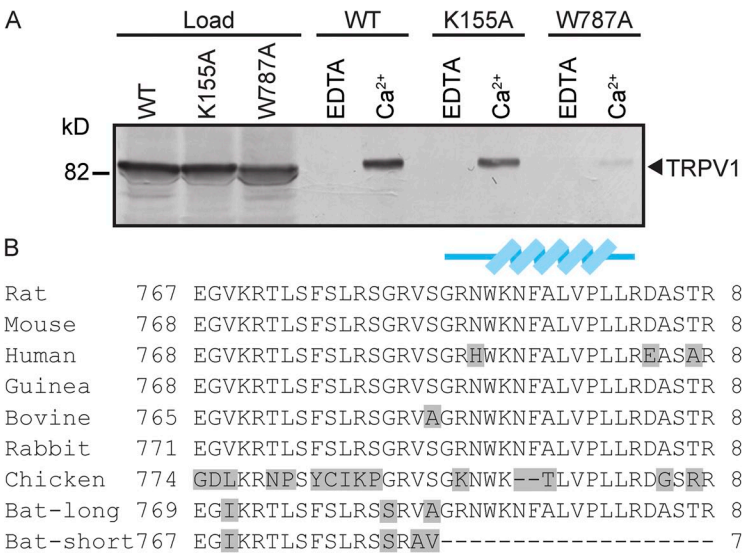

Figure 7. The conserved TRPV1-CT sequence is necessary for interaction of full-length TRPV1 with Ca^{2+}–CaM. (A) Tryptophan 787 is necessary for the interaction of full-length TRPV1 with Ca^{2+}–CaM. Detergent-soluble fractions of HEK293 cells expressing wild-type, K155A, or W787A FLAG-tagged TRPV1 were incubated with CaM-agarose beads in the presence of EDTA or $CaCl_2$ and washed, and the bound fractions were eluted and analyzed by Western blot using anti-FLAG antibody. Shown is a representative result of three independent experiments. (B) Sequence alignment of the rat TRPV1-CT35 region with representative mammalian and avian species shows that the region is highly conserved (sequence identity over the whole protein sequence of rat TRPV1 vs. mouse, human, guinea pig, bovine, rabbit, chicken, and bat splice variants [long and short] TRPV1 is 96, 86, 89, 86, 87, 67, 86, and 87%, respectively). Nonconserved residues are shaded gray. The region visible in the crystal structure (residues 784–798) and the helical region (788–796) are indicated above the alignment (cyan).

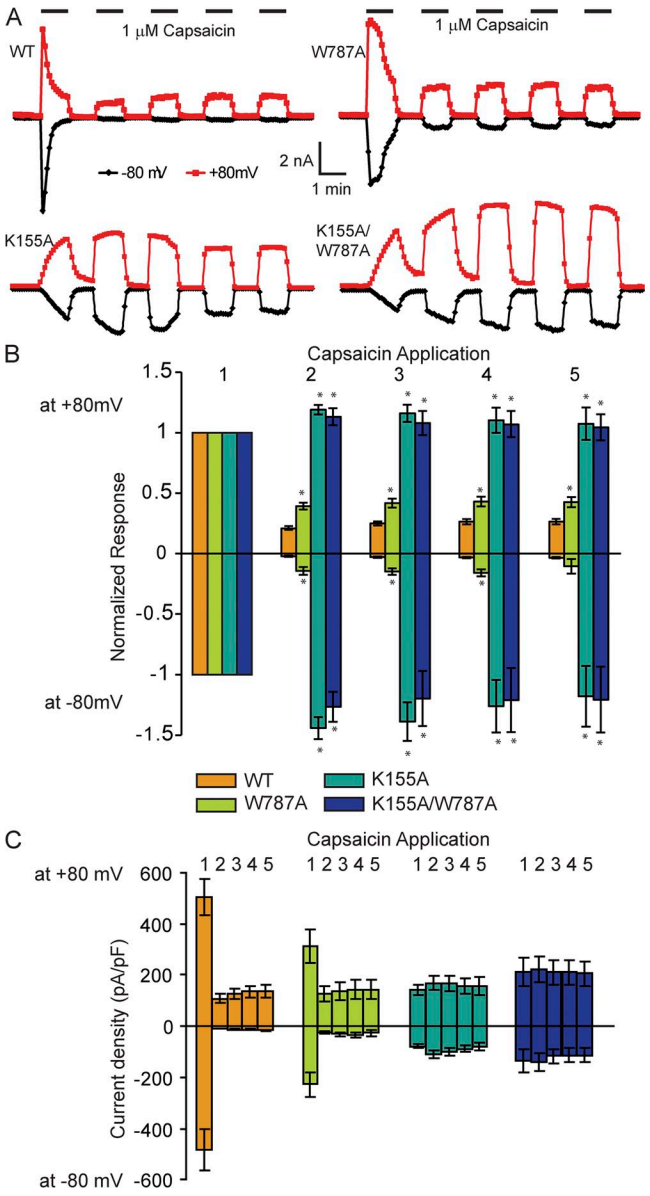

Figure 8. Mutations that reduce CaM binding to the TRPV1-ARD or TRPV1-CT caused different defects in TRPV1 current desensitization in HEK293 cells. (A) Representative traces of capsaicin-evoked whole cell currents in response to repeated capsaicin applications in the presence of extracellular Ca^{2+}. Cells were repeatedly stimulated with 1 μM capsaicin for 1 min followed by 1-min washouts. The +80 mV (red) and −80 mV (black) currents extracted from 1,500-ms voltage ramps are shown. (B) Mean current amplitudes for successive capsaicin applications were normalized to the maximal current amplitudes of the first capsaicin application. *, $P < 0.01$ versus TRPV1 wild type using two-tailed unpaired *t* tests. (C) Mean current density of the maximal response to the first capsaicin application normalized to the cell capacitance. The values in B and C were calculated from current amplitudes at −80 mV (negative scale) and +80 mV (positive scale) measured in experiments as in A. Bars represent mean ± SEM ($n = 6, 8, 8$, and 8 for wild type, W787A, K155A, and W787A/K155A, respectively).

The TRPV1-CT Ca^{2+}–CaM-binding site identified in our structure overlaps a region previously identified as an inhibitory PIP_2-binding domain, although no direct binding was demonstrated (Prescott and Julius, 2003). A subsequent study found that the inhibitory effects of PIP_2 on TRPV1 were only detectable in whole cells, not excised patches, suggesting that PIP_2-mediated inhibition is indirect (Lukacs et al., 2007). Furthermore, PIP_2 can also potentiate TRPV1 (Liu et al., 2005; Lishko et al., 2007; Lukacs et al., 2007) and does so through a proximal CT region (residues 682–725) (Ufret-Vincenty et al., 2011). Together with these findings on TRPV1 regulation by PIP_2, our data support the distal CT region of TRPV1 as a physiologically important Ca^{2+}–CaM-binding site.

The interactions of Ca^{2+}–CaM with both TRPV1-ARD and TRPV1-CT are implicated in TRPV1 desensitization (Numazaki et al., 2003; Lishko et al., 2007). This brings up the question of whether Ca^{2+}–CaM regulation of TRPV1 at TRPV1-ARD and TRPV1-CT constitutes integrated or separate mechanisms. Several findings suggested that both sites may work together in the desensitization mechanism. First, mutations or deletion of the Ca^{2+}–CaM-binding site either in TRPV1-ARD or TRPV1-CT disrupts desensitization (Numazaki et al., 2003; Lishko et al., 2007). Second, a toxicity-based screen for active or hypersensitive TRPV1 phenotype (Myers et al., 2008) identified mutations that impair Ca^{2+}–CaM binding in either TRPV1-ARD, such as K155E/A and K160E/A (Lishko et al., 2007), or TRPV1-CT, such as W787R and L792P (Fig. 3 C). One hypothesis is that Ca^{2+}–CaM may bridge an interaction between TRPV1-ARD and TRPV1-CT (Lishko et al., 2007). A similar mechanism is postulated for CaM regulation of voltage-gated Ca_v1 channels (Dick et al., 2008), and CaM bridges two subunits of a Ca^{2+}-activated K^+ channel (Schumacher et al., 2001). Here, we generated two different cross-linked Ca^{2+}-CaM–TRPV1-CT complexes but did not observe any ternary assemblies of these cross-linked complexes with TRPV1-ARD. This suggests that the Ca^{2+}–CaM-mediated desensitization of TRPV1 may instead involve separate pathways. However, we cannot rule out the possibility that the introduced cross-links, which maintain the interactions observed in the un–cross-linked complex (Fig. S5), may restrict conformational changes required for interaction with TRPV1-ARD.

We observed a more pronounced disruption of desensitization in response to capsaicin when mutating the N-terminal K155A than the CT W787A, suggesting that the TRPV1-ARD is most important for tachyphylaxis. Mutation of the CT site, on the other hand, led to a more subtle phenotype of slowed and reduced desensitization (Fig. 8). Notably, the CT site was most important for Ca^{2+}–CaM binding in our pulldown assays. Therefore, our data suggest that Ca^{2+}–CaM binding may

not be the dominant regulatory factor for TRPV1 desensitization. Overall, our data are consistent with a model where PIP_2 depletion is a major contributor to the acute desensitization of TRPV1 after activation by capsaicin (Lukacs et al., 2007; Mercado et al., 2010), with Ca^{2+}–CaM binding to the TRPV1-CT likely playing a supporting role.

It is possible that the CT Ca^{2+}–CaM-binding site plays a more important role in regulating other TRPV1 responses not tested in the current study. Several studies hint at a role of the TRPV1-CT Ca^{2+}–CaM-binding site in tuning channel sensitivity. Increased sensitivity to heat and/or hypersensitivity was observed in several CT mutants (Prescott and Julius, 2003; Myers et al., 2008) and in the vampire bat TRPV1-S isoform in which the CT-binding site is absent (Gracheva et al., 2011).

In summary, we showed that TRPV1-CT represents a high affinity binding site for Ca^{2+}–CaM. The TRPV1-ARD and TRPV1-CT likely provide two separate regulatory pathways, a model that is supported by both our biochemical and electrophysiological analyses. Our work provides new biochemical and structural information that enables future studies to fully decipher the molecular mechanisms behind the physiological regulation of TRPV1 responses.

We thank current and former laboratory members for technical help and discussions. Special thanks to Wilhelm Weihofen for advice and assistance on x-ray crystallography; Marcos Sotomayor and Ahmet Vakkasoglu for x-ray data collection; Alejandra Beristain-Barajas for technical assistance; and Hitoshi Inada for assistance with electrophysiology, discussions, and insights to this work. We are grateful to Narayanasami Sukumar and staff at the Northeastern Collaborative Access Team (NE-CAT), beamline 24-ID-C, for assistance with data collection.

This work was supported by National Institutes of Health (NIH; grant R01GM081340) and Klingenstein Awards to R. Gaudet. Use of APS beamlines was supported by NIH award RR-15301 and Department of Energy contract DE-AC02-06CH11357.

Edward N. Pugh Jr. served as editor.

Submitted: 28 March 2012
Accepted: 4 October 2012

REFERENCES

Aoyagi, M., A.S. Arvai, J.A. Tainer, and E.D. Getzoff. 2003. Structural basis for endothelial nitric oxide synthase binding to calmodulin. *EMBO J.* 22:766–775. http://dx.doi.org/10.1093/emboj/cdg078

Ataman, Z.A., L. Gakhar, B.R. Sorensen, J.W. Hell, and M.A. Shea. 2007. The NMDA receptor NR1 C1 region bound to calmodulin: structural insights into functional differences between homologous domains. *Structure.* 15:1603–1617. http://dx.doi.org/10.1016/j.str.2007.10.012

Baker, N.A., D. Sept, S. Joseph, M.J. Holst, and J.A. McCammon. 2001. Electrostatics of nanosystems: application to microtubules and the ribosome. *Proc. Natl. Acad. Sci. USA.* 98:10037–10041. http://dx.doi.org/10.1073/pnas.181342398

Barbato, G., M. Ikura, L.E. Kay, R.W. Pastor, and A. Bax. 1992. Backbone dynamics of calmodulin studied by 15N relaxation using inverse detected two-dimensional NMR spectroscopy: the central helix is flexible. *Biochemistry.* 31:5269–5278. http://dx.doi.org/10.1021/bi00138a005

Bhave, G., H.J. Hu, K.S. Glauner, W. Zhu, H. Wang, D.J. Brasier, G.S. Oxford, and R.W. Gereau IV. 2003. Protein kinase C phosphorylation sensitizes but does not activate the capsaicin receptor transient receptor potential vanilloid 1 (TRPV1). *Proc. Natl. Acad. Sci. USA.* 100:12480–12485. http://dx.doi.org/10.1073/pnas.2032100100

Bogan, A.A., and K.S. Thorn. 1998. Anatomy of hot spots in protein interfaces. *J. Mol. Biol.* 280:1–9. http://dx.doi.org/10.1006/jmbi.1998.1843

Caterina, M.J., M.A. Schumacher, M. Tominaga, T.A. Rosen, J.D. Levine, and D. Julius. 1997. The capsaicin receptor: a heat-activated ion channel in the pain pathway. *Nature.* 389:816–824. http://dx.doi.org/10.1038/39807

Clapperton, J.A., S.R. Martin, S.J. Smerdon, S.J. Gamblin, and P.M. Bayley. 2002. Structure of the complex of calmodulin with the target sequence of calmodulin-dependent protein kinase I: studies of the kinase activation mechanism. *Biochemistry.* 41:14669–14679. http://dx.doi.org/10.1021/bi026660t

Crivici, A., and M. Ikura. 1995. Molecular and structural basis of target recognition by calmodulin. *Annu. Rev. Biophys. Biomol. Struct.* 24:85–116. http://dx.doi.org/10.1146/annurev.bb.24.060195.000505

Dick, I.E., M.R. Tadross, H. Liang, L.H. Tay, W. Yang, and D.T. Yue. 2008. A modular switch for spatial Ca2+ selectivity in the calmodulin regulation of CaV channels. *Nature.* 451:830–834. http://dx.doi.org/10.1038/nature06529

Docherty, R.J., J.C. Yeats, S. Bevan, and H.W. Boddeke. 1996. Inhibition of calcineurin inhibits the desensitization of capsaicin-evoked currents in cultured dorsal root ganglion neurones from adult rats. *Pflugers Arch.* 431:828–837.

Drum, C.L., Y. Shen, P.A. Rice, A. Bohm, and W.J. Tang. 2001. Crystallization and preliminary X-ray study of the edema factor exotoxin adenylyl cyclase domain from Bacillus anthracis in the presence of its activator, calmodulin. *Acta Crystallogr. D Biol. Crystallogr.* 57:1881–1884. http://dx.doi.org/10.1107/S0907444901014937

Emsley, P., and K. Cowtan. 2004. Coot: model-building tools for molecular graphics. *Acta Crystallogr. D Biol. Crystallogr.* 60:2126–2132. http://dx.doi.org/10.1107/S0907444904019158

Gaudet, R. 2008. TRP channels entering the structural era. *J. Physiol.* 586:3565–3575. http://dx.doi.org/10.1113/jphysiol.2008.155812

Gomes, A.V., J.A. Barnes, and H.J. Vogel. 2000. Spectroscopic characterization of the interaction between calmodulin-dependent protein kinase I and calmodulin. *Arch. Biochem. Biophys.* 379:28–36. http://dx.doi.org/10.1006/abbi.2000.1827

Gordon-Shaag, A., W.N. Zagotta, and S.E. Gordon. 2008. Mechanism of Ca(2+)-dependent desensitization in TRP channels. *Channels (Austin).* 2:125–129. http://dx.doi.org/10.4161/chan.2.2.6026

Gracheva, E.O., J.F. Cordero-Morales, J.A. González-Carcacía, N.T. Ingolia, C. Manno, C.I. Aranguren, J.S. Weissman, and D. Julius. 2011. Ganglion-specific splicing of TRPV1 underlies infrared sensation in vampire bats. *Nature.* 476:88–91. http://dx.doi.org/10.1038/nature10245

Grycova, L., Z. Lansky, E. Friedlova, V. Obsilova, H. Janouskova, T. Obsil, and J. Teisinger. 2008. Ionic interactions are essential for TRPV1 C-terminus binding to calmodulin. *Biochem. Biophys. Res. Commun.* 375:680–683. http://dx.doi.org/10.1016/j.bbrc.2008.08.094

Han, P., H.A. McDonald, B.R. Bianchi, R.E. Kouhen, M.H. Vos, M.F. Jarvis, C.R. Faltynek, and R.B. Moreland. 2007. Capsaicin causes protein synthesis inhibition and microtubule disassembly through TRPV1 activities both on the plasma membrane and intracellular membranes. *Biochem. Pharmacol.* 73:1635–1645. http://dx.doi.org/10.1016/j.bcp.2006.12.035

Hazes, B., and B.W. Dijkstra. 1988. Model building of disulfide bonds in proteins with known three-dimensional structure. *Protein Eng.* 2:119–125. http://dx.doi.org/10.1093/protein/2.2.119

Hoeflich, K.P., and M. Ikura. 2002. Calmodulin in action: diversity in target recognition and activation mechanisms. *Cell.* 108:739–742. http://dx.doi.org/10.1016/S0092-8674(02)00682-7

Ikura, M., G.M. Clore, A.M. Gronenborn, G. Zhu, C.B. Klee, and A. Bax. 1992. Solution structure of a calmodulin-target peptide complex by multidimensional NMR. *Science.* 256:632–638. http://dx.doi.org/10.1126/science.1585175

Karai, L., D.C. Brown, A.J. Mannes, S.T. Connelly, J. Brown, M. Gandal, O.M. Wellisch, J.K. Neubert, Z. Olah, and M.J. Iadarola. 2004. Deletion of vanilloid receptor 1-expressing primary afferent neurons for pain control. *J. Clin. Invest.* 113:1344–1352.

Kim, E.Y., C.H. Rumpf, Y. Fujiwara, E.S. Cooley, F. Van Petegem, and D.L. Minor Jr. 2008. Structures of CaV2 Ca2+/CaM-IQ domain complexes reveal binding modes that underlie calcium-dependent inactivation and facilitation. *Structure.* 16:1455–1467. http://dx.doi.org/10.1016/j.str.2008.07.010

Kurokawa, H., M. Osawa, H. Kurihara, N. Katayama, H. Tokumitsu, M.B. Swindells, M. Kainosho, and M. Ikura. 2001. Target-induced conformational adaptation of calmodulin revealed by the crystal structure of a complex with nematode Ca(2+)/calmodulin-dependent kinase kinase peptide. *J. Mol. Biol.* 312:59–68. http://dx.doi.org/10.1006/jmbi.2001.4822

Lishko, P.V., E. Procko, X. Jin, C.B. Phelps, and R. Gaudet. 2007. The ankyrin repeats of TRPV1 bind multiple ligands and modulate channel sensitivity. *Neuron.* 54:905–918. http://dx.doi.org/10.1016/j.neuron.2007.05.027

Liu, B., C. Zhang, and F. Qin. 2005. Functional recovery from desensitization of vanilloid receptor TRPV1 requires resynthesis of phosphatidylinositol 4,5-bisphosphate. *J. Neurosci.* 25:4835–4843. http://dx.doi.org/10.1523/JNEUROSCI.1296-05.2005

Lukacs, V., B. Thyagarajan, P. Varnai, A. Balla, T. Balla, and T. Rohacs. 2007. Dual regulation of TRPV1 by phosphoinositides. *J.Neurosci.*27:7070–7080.http://dx.doi.org/10.1523/JNEUROSCI.1866-07.2007

Meador, W.E., A.R. Means, and F.A. Quiocho. 1992. Target enzyme recognition by calmodulin: 2.4 A structure of a calmodulin-peptide complex. *Science.* 257:1251–1255. http://dx.doi.org/10.1126/science.1519061

Meador, W.E., A.R. Means, and F.A. Quiocho. 1993. Modulation of calmodulin plasticity in molecular recognition on the basis of x-ray structures. *Science.* 262:1718–1721. http://dx.doi.org/10.1126/science.8259515

Mercado, J., A. Gordon-Shaag, W.N. Zagotta, and S.E. Gordon. 2010. Ca2+-dependent desensitization of TRPV2 channels is mediated by hydrolysis of phosphatidylinositol 4,5-bisphosphate. *J. Neurosci.* 30:13338–13347. http://dx.doi.org/10.1523/JNEUROSCI.2108-10.2010

Mohapatra, D.P., and C. Nau. 2005. Regulation of Ca2+-dependent desensitization in the vanilloid receptor TRPV1 by calcineurin and cAMP-dependent protein kinase. *J. Biol. Chem.* 280:13424–13432. http://dx.doi.org/10.1074/jbc.M410917200

Mohapatra, D.P., S.Y. Wang, G.K. Wang, and C. Nau. 2003. A tyrosine residue in TM6 of the Vanilloid Receptor TRPV1 involved in desensitization and calcium permeability of capsaicin-activated currents. *Mol. Cell. Neurosci.* 23:314–324. http://dx.doi.org/10.1016/S1044-7431(03)00054-X

Murshudov, G.N., A.A. Vagin, and E.J. Dodson. 1997. Refinement of macromolecular structures by the maximum-likelihood method. *Acta Crystallogr. D Biol. Crystallogr.* 53:240–255. http://dx.doi.org/10.1107/S0907444996012255

Myers, B.R., C.J. Bohlen, and D. Julius. 2008. A yeast genetic screen reveals a critical role for the pore helix domain in TRP channel gating. *Neuron.* 58:362–373. http://dx.doi.org/10.1016/j.neuron.2008.04.012

Numazaki, M., T. Tominaga, K. Takeuchi, N. Murayama, H. Toyooka, and M. Tominaga. 2003. Structural determinant of TRPV1 desensitization interacts with calmodulin. *Proc. Natl. Acad. Sci. USA.* 100:8002–8006. http://dx.doi.org/10.1073/pnas.1337252100

Osawa, M., H. Tokumitsu, M.B. Swindells, H. Kurihara, M. Orita, T. Shibanuma, T. Furuya, and M. Ikura. 1999. A novel target recognition revealed by calmodulin in complex with Ca2+-calmodulin-dependent kinase kinase. *Nat. Struct. Biol.* 6:819–824. http://dx.doi.org/10.1038/12271

Otwinowski, Z., and W. Minor. 1997. Processing of X-ray diffraction data collected in oscillation mode: Methods in Enzymology. *In* Macromolecular Crystallography Part A. J.C.W. Carter, editor. Academic Press, New York. 307–326.

Phelps, C.B., E. Procko, P.V. Lishko, R.R. Wang, and R. Gaudet. 2007. Insights into the roles of conserved and divergent residues in the ankyrin repeats of TRPV ion channels. *Channels (Austin).* 1:148–151.

Prescott, E.D., and D. Julius. 2003. A modular PIP2 binding site as a determinant of capsaicin receptor sensitivity. *Science.* 300:1284–1288. http://dx.doi.org/10.1126/science.1083646

Rhoads, A.R., and F. Friedberg. 1997. Sequence motifs for calmodulin recognition. *FASEB J.* 11:331–340.

Rosenbaum, T., M. Awaya, and S.E. Gordon. 2002. Subunit modification and association in VR1 ion channels. *BMC Neurosci.* 3:4. http://dx.doi.org/10.1186/1471-2202-3-4

Rosenbaum, T., A. Gordon-Shaag, M. Munari, and S.E. Gordon. 2004. Ca^{2+}/calmodulin modulates TRPV1 activation by capsaicin. *J. Gen. Physiol.* 123:53–62. http://dx.doi.org/10.1085/jgp.200308906

Schägger, H. 2006. Tricine-SDS-PAGE. *Nat. Protoc.* 1:16–22. http://dx.doi.org/10.1038/nprot.2006.4

Schumacher, M.A., A.F. Rivard, H.P. Bächinger, and J.P. Adelman. 2001. Structure of the gating domain of a Ca2+-activated K+ channel complexed with Ca2+/calmodulin. *Nature.* 410:1120–1124. http://dx.doi.org/10.1038/35074145

Stein, A.T., C.A. Ufret-Vincenty, L. Hua, L.F. Santana, and S.E. Gordon. 2006. Phosphoinositide 3-kinase binds to TRPV1 and mediates NGF-stimulated TRPV1 trafficking to the plasma membrane. *J. Gen. Physiol.* 128:509–522. http://dx.doi.org/10.1085/jgp.200609576

Tjandra, N., H. Kuboniwa, H. Ren, and A. Bax. 1995. Rotational dynamics of calcium-free calmodulin studied by 15N-NMR relaxation measurements. *Eur. J. Biochem.* 230:1014–1024. http://dx.doi.org/10.1111/j.1432-1033.1995.tb20650.x

Tominaga, M., M.J. Caterina, A.B. Malmberg, T.A. Rosen, H. Gilbert, K. Skinner, B.E. Raumann, A.I. Basbaum, and D. Julius. 1998. The cloned capsaicin receptor integrates multiple pain-producing stimuli. *Neuron.* 21:531–543. http://dx.doi.org/10.1016/S0896-6273(00)80564-4

Ufret-Vincenty, C.A., R.M. Klein, L. Hua, J. Angueyra, and S.E. Gordon. 2011. Localization of the PIP2 sensor of TRPV1 ion channels. *J. Biol. Chem.* 286:9688–9698. http://dx.doi.org/10.1074/jbc.M110.192526

Vetter, S.W., and E. Leclerc. 2003. Novel aspects of calmodulin target recognition and activation. *Eur. J. Biochem.* 270:404–414. http://dx.doi.org/10.1046/j.1432-1033.2003.03414.x

Weljie, A.M., and H.J. Vogel. 2000. Tryptophan fluorescence of calmodulin binding domain peptides interacting with calmodulin containing unnatural methionine analogues. *Protein Eng.* 13:59–66. http://dx.doi.org/10.1093/protein/13.1.59

Yamauchi, E., T. Nakatsu, M. Matsubara, H. Kato, and H. Taniguchi. 2003. Crystal structure of a MARCKS peptide containing the calmodulin-binding domain in complex with Ca2+-calmodulin. *Nat. Struct. Biol.* 10:226–231. http://dx.doi.org/10.1038/nsb900

Yamniuk, A.P., and H.J. Vogel. 2004. Calmodulin's flexibility allows for promiscuity in its interactions with target proteins and peptides. *Mol. Biotechnol.* 27:33–57. http://dx.doi.org/10.1385/MB:27:1:33

Yao, J., and F. Qin. 2009. Interaction with phosphoinositides confers adaptation onto the TRPV1 pain receptor. *PLoS Biol.* 7:e46. http://dx.doi.org/10.1371/journal.pbio.1000046

Zhang, X., L. Li, and P.A. McNaughton. 2008. Proinflammatory mediators modulate the heat-activated ion channel TRPV1 via the scaffolding protein AKAP79/150. *Neuron.* 59:450–461. http://dx.doi.org/10.1016/j.neuron.2008.05.015

Zhu, M.X. 2005. Multiple roles of calmodulin and other Ca(2+)-binding proteins in the functional regulation of TRP channels. *Pflugers Arch.* 451:105–115. http://dx.doi.org/10.1007/s00424-005-1427-1